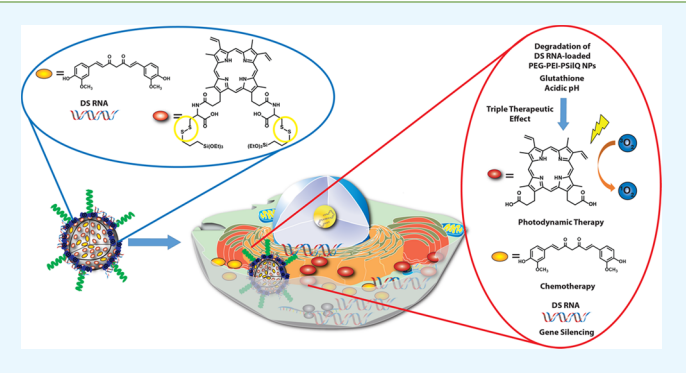
Multimodal Polysilsesquioxane Nanoparticles for Combinatorial Therapy and Gene Delivery in Triple-Negative Breast Cancer

Ridhima Juneja, † Dachary Lyles, † Demapriyadarshini Vadarevu, † Kirill A. Afonin, † Hemapriyadarshini Vadarevu, † Kirill A. Afonin, † Demapriyadarshini Vadarevu, † Demapriyadarshini Vad

[†]Department of Chemistry, [‡]The Centre for Biomedical Engineering and Science, and [§]Nanoscale Science Program, University of North Carolina at Charlotte, Charlotte, North Carolina 28223, United States

Supporting Information

ABSTRACT: Multifunctional hybrid nanoparticles are being developed to carry a wide variety of therapeutic and imaging agents for multiple biomedical applications. Polysilsesquioxane (PSilQ) nanoparticles are a promising hybrid platform with numerous advantages to be used as a delivery system. In this report, we demonstrate the ability of a stimuli-responsive PSilQ-based platform to transport and deliver simultaneously protoporphyrin IX, curcumin, and RNA interference inducers inside human cells. This multimodal delivery system shows a synergistic performance for the combined phototherapy and chemotherapy of triple-negative breast cancer and can be used for efficient transfection of therapeutic nucleic acids. The



current work represents the first report of using the PSilQ platform for the combined phototherapy and chemotherapy and gene delivery.

KEYWORDS: Polysilsesquioxane nanoparticles, Combination therapy, Photodynamic therapy, Stimuli-responsive systems, Gene delivery, Triple-negative breast cancer

1. INTRODUCTION

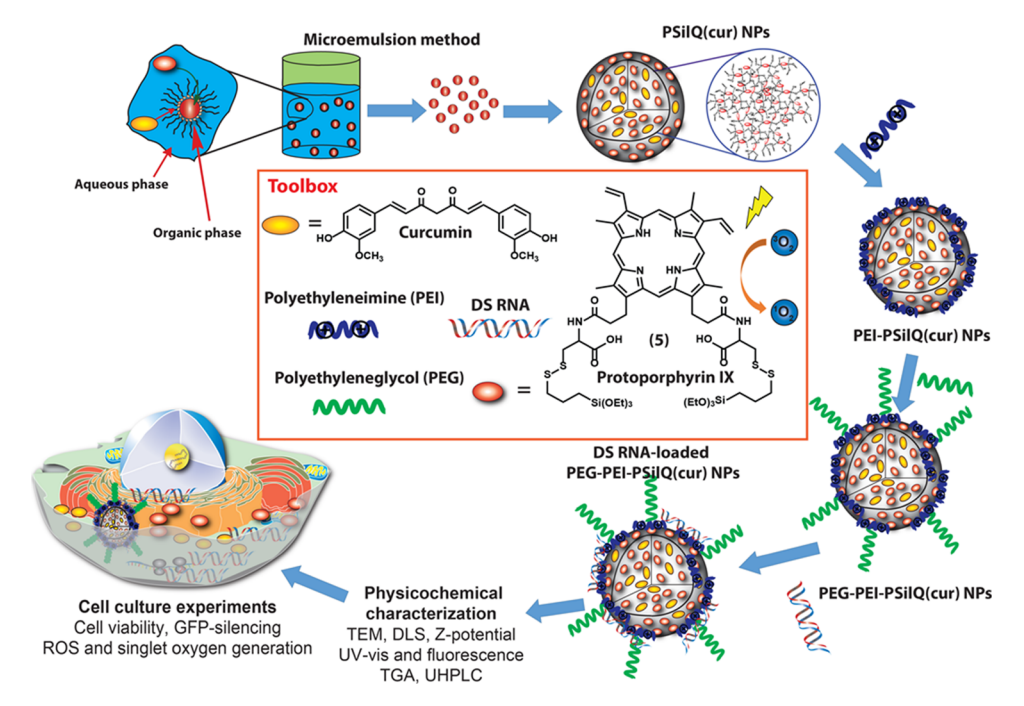
Hybrid nanoparticles designed with both inorganic and organic components have attracted great attention in the last decade because they not only retain the beneficial features of both components but also gain an additional synergistic performance. Hybrid nanomaterials can be modified in a modular fashion to render specific properties for the resultant nanoparticles such as target specificity or biodegradability.^{1,2} In the field of nanomedicine, a variety of hybrid nanoparticles such as nanoscale metal organic framework and silica-based and nanoscale coordination polymers have been investigated for drug delivery, biosensing, and imaging. 3-6 The silica-based hybrid nanoparticles known as polysilsesquioxane (PSilQ) nanoparticles have been recently introduced as a promising alternative for the efficient delivery of therapeutic agents. PSilQ-based platforms offer similar biocompatibility and chemical tunability as other silica-based materials but with much higher drug loading capacity and degradable features when compared to traditional silica-based nanoparticles. 6-8 Our group and others have developed PSilQ platforms for different therapeutic and imaging applications. Lin and coworkers reported the synthesis and characterization of PSilQ nanoparticles containing either cisplatin or gadolinium molecules for cancer chemotherapy or magnetic resonance imaging. 9,10 Durand and co-workers pioneered the use of PSilQ nanoparticles for near-infrared two-photon photodynamic therapy and imaging. 11,12 The same group recently

expanded the concept to include gene delivery. 13 Khashab and co-workers have also demonstrated the development of enzymatically degradable PSilQ nanomaterials for in vitro imaging.¹⁴ Our group has reported the synthesis of porphyrinbased PSilQ nanomaterials to improve the photodynamic therapy against cancer. 15,16 Our strategy consisted of developing porphyrin-based PSilQ nanoparticles with high loading of porphyrin and redox-responsive properties to enhance the delivery and biodegradability of the platform under a reducing environment inside cancer cells.1

Triple-negative breast cancer (TNBC) is a highly aggressive subtype of breast cancer. TNBC is characterized by intratumor heterogeneity, high proliferative activity, poor prognosis, high risk of relapse, and metastasis to the lungs and brain.¹⁸ The effective treatment of TNBC requires a multimodal approach that targets and inhibits multiple essential pathways of tumor growth, invasiveness, or metastasis. 19,20 Silica-based hybrid nanoparticles that carry either more than one chemotherapeutic drug or different types of therapeutic agents have shown promising results for the treatment of cancer. ^{21–23} The combination of chemotherapy with photodynamic therapies and/or gene therapy is expected to improve the treatment of TNBC. Herein, we report the design, synthesis, character-

Received: January 12, 2019 Accepted: March 7, 2019 Published: March 7, 2019

Scheme 1. Schematic Representation of the Synthesis and Characterization of the GFP-DS RNA-Loaded PEG-PEI-PSilQ(cur) Platform^a



"PpIX is part of the framework of the PSilQ system chemically bound through disulfide and silica bonds (5) (PSilQ NPs). Curcumin is encapsulated during the microemulsion reaction to fabricate PSilQ(cur) NPs. The surface PSilQ(cur) NPs are further functionalized with PEI and PEG to afford PEG-PEI-PSilQ(cur) and PEI-PSilQ(cur) NPs. GFP-DS RNA is electrostatically attached to the PEG-PEI-PSilQ(cur) NPs. The physicochemical properties of the PSilQ(cur) materials such as TEM, DLS, ζ -potential, UV—vis and fluorescence spectroscopy, TGA, and UHPLC analysis are evaluated. The in vitro performances including the combined phototherapy and chemotherapy, GFP silencing, ROS, and ¹O₂ generation of the GFP-DS RNA-loaded PEG-PEI-PSilQ(cur) NP platform are determined using MDA-MB-231 cells.

ization, and in vitro application of a stimuli-responsive multimodal porphyrin-based PSilQ platform that effectively combines all three aforementioned therapies.

The PSilQ platform, shown in Scheme 1, consists of the redox-responsive protoporphyrin IX (PpIX) silane derivative 5 as the building unit for the PSilO network (PSilO NPs). PpIX is a well-known PS that has great potential for use in PDT. However, PpIX is poorly soluble in physiological conditions and cannot be administered intravenously directly.²⁴ Therefore, improvement in the PDT efficacy can be achieved by incorporating PpIX molecules into PSilQ NPs. Moreover, compound 5 was rationally designed to include a redoxresponsive linker (Scheme 1 and Scheme S3), a disulfide bond, which is selectively cleaved in the presence of a high reducing environment such as that found inside cancer cells.²⁵ These nanoparticles are also loaded with curcumin (PSilQ(cur) NPs), which exhibits pharmacological properties against several diseases including cancer, oxidative stress, aging, inflammation, and microbial infection.²⁶ Curcumin has shown good anticancer activity against TNBC.^{27,28} The surface of the PSilQ(cur) NPs was modified with polyethyleneimine (PEI, MW = 10 kDa) and polyethylene glycol (PEG, MW = 2 kDa) to afford PEG-PEI-PSilQ(cur) and PEI-PSilQ(cur) NPs. The first RNA interference (RNAi) therapeutic agent (patisiran) has been approved by the FDA for clinical applications in 2018.²⁹ Therefore, there is an increasing demand in developing clinically relevant nanoformulations with a high level of silencing efficiencies. Dicer substrate (DS) RNAs, used in this work as RNAi inducers, 30 were designed for a Dicer-assisted release of siRNAs that further silence green fluorescent protein (GFP) expression. In this work, PSilQ NPs

with high loading of PpIX and curcumin were synthesized and further modified to be suitable for efficient DS RNA delivery (GFP-DS RNA-loaded PEG-PEI-PSilQ(cur) NPs). Spherical nanoparticles with a diameter size of 40 \pm 5 nm and high loading of PpIX (24.4 \pm 2.5 wt %) and curcumin (7.6 \pm 1.5 wt %) were obtained. The combined therapeutic effect of the PSilQ(cur) NPs was evaluated against MDA-MB-231 cells. A synergistic therapeutic effect was observed in the combination of PpIX and curcumin. The PSilQ platform was more selective toward MDA-MB-231 than the healthy breast MCF-10a cells compared with PpIX. In addition, GFP-DS RNA transfection studies showed significant GFP silencing when tested in MDA-MB-231/GFP cells. Our results demonstrate the potential of the PSilQ platform to be used for combinatorial therapy of TNBC as well as a delivery vector for therapeutic nucleic acids.

2. EXPERIMENTAL SECTION

2.1. Synthesis of PSilQ and PSilQ(cur) Nanoparticles. The direct microemulsion method was used as the approach for the synthesis of PpIX-based redox-responsive PSilQ nanoparticles (Scheme 1). The following procedure was followed: 0.22 g of dioctyl sulfosuccinate sodium salt (0.495 mmol) was added to 10 mL of nanopure water under gentle stirring for 30 min at room temperature, which gave a translucent solution. Then, 0.4 mL of n-butanol was added. Once the solution became clear, 0.1 mL of cyclohexane (oil phase) was added. The final mixture was allowed to stir for 15 min to give a single-phase transparent solution. To this mixture, a solution of ligand 5 (1.6 mg) in 1:2 dimethyl sulfoxide/dimethyl formamide mixture (0.1 mL) was added dropwise under continuous stirring at room temperature. The synthesis of compound 5 is depicted in Scheme S1 (Supporting Information). To promote the solubility and condensation process of ligand 5, 0.1 mL of aqueous ammonia (28%)

followed by 0.2 mL of an aqueous solution of NaOH (2 M) was added to the solution. The reaction mixture was allowed to stir for 48 h at room temperature. The nanoparticles were obtained by disrupting the microemulsion with an excess of acetone, which afforded the precipitation of the PSilO NPs as dark brown precipitate. The PSilQ NPs were collected by centrifugation (13,000 rpm for 10 min) and washed sequentially with acetone, ethanol, and dimethyl formamide to remove any unreacted reagents. The washed PSilQ NPs were stored in ethanol at 4 °C.

Curcumin was used as a model drug for encapsulation into the hydrophobic core of the PSilQ NPs. To synthesize this material, 0.4 mL of curcumin solution (5 mg/mL in dimethyl sulfoxide) was added to the oil-in-water microemulsion described above before the addition of the PpIX-based ligand 5. The resultant PSilQ(cur) NPs were collected by centrifugation and washed with different solvents, as described above. The washed PSilQ(cur) NPs were stored in ethanol at 4 °C. The supernatant and washing solutions were stored to quantify the loading of curcumin using ultrahigh-performance liquid chromatography (UHPLC).

- 2.2. Modification of PSilQ(cur) Nanoparticles with Polyethyleneimine (PEI) Polymer. To modify the surface of PSilQ(cur) NPs with a PEI polymer (MW = 10 kDa), 10 mg of PSilQ(cur) NPs was redispersed in 1.0 mL of nanopure water. PEI solution (5 mg of PEI in 0.25 mL of ethanol) was added dropwise to the nanoparticle dispersion under gentle stirring at room temperature for 2 h. The PEI-PSilQ(cur) NPs were collected by centrifugation (15,000 rpm for 10 min) and washed three times with ethanol to remove the excess of PEI. The final PEI-PSilQ(cur) NPs were stored in ethanol at 4 °C. The amount of amine groups chemically available on the surface of PEI-PSilQ(cur) NPs was indirectly quantified by using the Kaiser's test.31
- 2.3. Functionalization of PEI-PSilQ(cur) Nanoparticles with **Polyethylene glycol (PEG) Polymer.** PEI-PSilQ(cur) NPs were further functionalized with a PEG (MW = 2 kDa) polymer, as shown in Scheme 1. For this, 10 mg of PEI-PSilQ(cur) NPs was redispersed in 9 mL of ethanol. To this dispersion, an ethanolic solution of bifunctional methoxy/succinic anhydride PEG polymer (3 mg in 1 mL of ethanol) was added dropwise under stirring conditions. The reaction mixture was allowed to stir for 24 h at room temperature. The PEG-PEI-PSilQ(cur) NPs were collected by centrifugation (15,000 rpm for 10 min) and washed twice with ethanol to remove any unreacted bifunctional PEG polymer. The PEG-PEI-PSilQ(cur) NPs were redispersed and stored in ethanol at 4 °C. The amount of amine groups chemically available on the surface of PEG-PEI-PSilQ(cur) NPs was indirectly quantified using the Kaiser's test.³¹
- 2.4. Release of PpIX from PSiIQ NPs in a Reducing Environment. As a proof of concept, the release of PpIX molecules from PSilQ NPs was investigated under a simulated reducing environment. Three separate dispersions of PSilQ NPs at a concentration of 2 mg/mL in 5 mL of dimethyl formamide were used. Before starting the time-dependent measurements, the PSilQ NPs were washed several times with dimethyl formamide to remove any physisorbed PpIX. Then, the dispersion of nanoparticles was stirred at 37 °C, and after regular time intervals of 30 min, the nanoparticles were centrifuged down, and the absorbance of the supernatant was measured at 408 nm. The supernatant was returned to the original vial, and the nanoparticles were redispersed. This process was repeated four times to determine the background release of PpIX. After that, dithiothreitol was added to two of the nanoparticle dispersions to reach a final concentration of 10 μM and 10 mM. The absorbance was measured at defined intervals of time (0-28 h) following the protocol described above. The values of absorbance were used to calculate and plot the percentage of PpIX release versus time. The PSilQ NP dispersion not treated with dithiothreitol was used as the control experiment. The data are presented as the average \pm SD of three independent experiments.
- 2.5. Measurement of Intracellular Reactive Oxygen Species. 2',7'-Dichlorodihydrofluorescein diacetate (DCFH-DA) is a commonly used cell-permeable fluorescent probe for measuring intracellular reactive oxygen species (ROS).³² MDA-MB-231 cells were

seeded in a 24-well plate at a density of 2×10^4 cells and incubated at 37 °C in 5% CO₂ atmosphere for 24 h. The cells were incubated for 24 h with PSilQ NPs or PSilQ(cur) NPs, each at three different concentrations of PpIX (22.0, 44.0, and 66.0 μ M). One hour before irradiation, the cell media were removed, and the cells were washed twice with phosphate buffer solution. MDA-MB-231 cells were incubated with 100 μ L of DCFH-DA (10 μ M) in low-serum (1 vol %) media in the dark at 37 °C and 5% CO₂. Subsequently, the media were removed, and the cells were washed with phosphate buffer solution. MDA-MB-231 cells were exposed to red light (630 nm, 24.5 mW/cm²) for 20 min. Immediately after irradiation, the cells were washed with phosphate buffer solution and harvested using trypsin. The formation of 2',7'-dichlorofluorescein was quantified by monitoring fluorescence at 528 nm using a flow cytometer (BD LSRFortessa cell analyzer). Results were analyzed using FlowJo software. Cells not treated with nanoparticles but incubated with ROS probe solution acted as the control experiment for this study. The results are reported as the average ± SD of three independent experiments.

Intracellular ¹O₂ generated by PSilQ NPs or PSilQ(cur) NPs was quantified by an indirect method using the fluorescence of singlet oxygen sensor green (SOSG) in the cell lysate.³³ MDA-MB-231 cells were seeded in a 96-well plate at a density of 2×10^4 cells per well and incubated at 37 °C in 5% CO₂ atmosphere for 24 h. The preseeded MDA-MB-231 cells in a 96-well plate were treated with different PpIX concentrations (22.0, 44.0, and 66.0 μ M) of PSilQ NPs and PSilQ(cur) NPs and incubated for 48 h at 37 °C in 5% CO₂ atmosphere. After inoculation with nanoparticles, the cell media were removed, and the cells were washed twice with phosphate buffer solution to remove any non-internalized nanoparticles. Then, MDA-MB-231 cells were lysed by adding 20 μ L of 1% Triton X-100 to each well and incubated for 30 min. Meanwhile, a stock solution of ¹O₂ probe (5 mM) was prepared in methanol by dissolving a 100 μ g vial of SOSG molecules in 33 μ L of methanol. This solution was utilized to make working solutions of 50 μ M, which are used right after preparation. Once the 30 min incubation time has ended, 12 μ L of this working solution of ${}^{1}O_{2}$ probe (50 μ M) was added to each well for a final concentration of 5 μ M. The lysate-containing 96-well plates were illuminated with light ($\lambda = 630 \text{ nm}$; fluence rate, 24.5 mW/cm²) for 20 min. The absorbance and emission values for the lysates were measured at excitation/emission of 505/520 nm using a microplate reader. The following control groups were also evaluated: MDA-MB-231 cells incubated with PSilQ NPs or PSilQ(cur) NPs but not irradiated and cells not treated with NPs. The results are reported as the average \pm SD of three independent experiments.

2.6. Qualitative Analysis of Reactive Oxygen Species Generation by Confocal Laser Scanning Microscopy. MDA-MB-231 cells were seeded on the top of a cover glass in six-well plates at a density of 1×10^5 cells per well and incubated for 24 h at 37 °C in 5% CO2 atmosphere. The cells were treated with PSilQ(cur) NPs in 2 mL of fresh media at a concentration of 30 μ g/mL and incubated for another 48 h. After removing the cell media, cells were washed with phosphate buffer solution. The ROS probe (10 μ M) was added to the cells in low-serum media (1 vol %) and incubated for 30 min under dark conditions. Once cell media were removed, the cells were washed with phosphate buffer solution and exposed to red light irradiation (630 nm, 24.5 mW/cm²) for 20 min. After irradiation, the cells were washed with phosphate buffer solution and mounted for microscopy analysis. Images were acquired using an Olympus FluoView FV 1000 confocal laser scanning microscope.

We also used the transporting properties of the PSilQ platform for visualizing the intracellular formation of ¹O₂ in vitro. SOSG molecules were first loaded to the fabricated PSilQ(cur) materials. By using this strategy, the PSilQ(cur) NPs are utilized to carry PpIX and, additionally, SOSG molecules. To prepare PSilQ(cur) NPs loaded with SOSG, 1 mg of PSilQ(cur) NPs was dispersed in 1.0 mL of aqueous solution of SOSG (1.0 mM). The dispersion was stirred for 24 h under dark conditions. Afterward, the nanoparticles were washed two times with phosphate buffer solution to remove any free SOSG molecules before further use. The prepared SOSG-doped PSilQ(cur)

NPs were redispersed in phosphate buffer solution (1 mg/mL). For in vitro imaging, the preseeded cells were treated with PSilO(cur) NPs and SOSG-doped PSilQ(cur) NPs. MDA-MB-231 cells were seeded on the top of a cover glass in six-well plates at a density of 1×10^5 cells per well and incubated for 24 h at 37 °C in 5% CO₂ atmosphere. The cells were treated with PSilQ(cur) NPs and SOSG-doped PSilQ(cur) NPs in 2 mL of fresh media at a concentration of 5 μ g/ mL and incubated for another 48 h. Next, the cells treated with PSilQ(cur) NPs were further incubated for 1 h with SOSG solution at a final concentration of 5 μM in the well plate. For comparison, the concentration of ROS probe to incubate the cells was fixed at 5 µM for all the sets. Subsequently, cell media were removed, and the cells were washed with phosphate buffer solution and exposed to red light irradiation (630 nm, 24.5 mW/cm²) for 20 min. After irradiation, the cells were washed with phosphate buffer solution, incubated with fresh media, and mounted for microscopy analysis. Images were acquired using an Olympus FluoView FV 1000 confocal fluorescence microscope.

2.7. In Vitro Phototoxicity. The in vitro cytotoxicity and phototoxicity of PpIX, silica NPs, PSilQ NPs, PSilQ(cur) NPs, PEI-PSilQ(cur) NPs, and PEG-PEI-PSilQ(cur) NPs were tested by using the MTS assay. For this study, MDA-MB-231 cells were seeded in a 96-well plate at a density of 5×10^3 cells per well in 100 μ L of complete media and incubated at 37 °C in 5% CO₂ atmosphere for 24 h. After removing the cell culture medium, PpIX (in DMSO; 0.01 vol %), silica NPs, PSilQ NPs, PSilQ(cur) NPs, PEI-PSilQ(cur) NPs, and PEG-PEI-PSilQ(cur) NPs were dispersed in complete media and added to the MDA-MB-231 cells at different PpIX concentrations $(9-222 \mu M)$. The concentrations of silica NPs used for these experiments are shown in Table S2. After 48 h of incubation in the presence of PSilQ materials, the culture media were removed, and the cells were washed twice with phosphate buffer solution. MDA-MB-231 cells were illuminated with red light (630 nm) at a fluence rate of 24.5 mW/cm² for 20 min. Control experiments were maintained in the same conditions but in the dark for the same interval of time. After irradiation, the media were replaced with fresh media, and the cells were allowed to grow for an additional 24 h. To measure the phototoxic and dark toxicity effects, the treated MDA-MB-231 cells were subjected to cell viability assay using the Cell Titer 96 Aqueous solution assay. To perform the assay, the cell media were removed, and the cells were washed with phosphate buffer solution. Fresh media (100 μ L) together with 20 μ L of CellTiter were added into each well and incubated for 2-3 h at 37 °C in 5% CO₂ atmosphere. Cell viability (%) was calculated as follows: viability = $(A_{\text{sample}}/A_{\text{control}})$ \times 100%, where A_{sample} and A_{control} denote absorbance values of the sample and control wells measured at 490 nm, respectively. The results are reported as the average \pm SD of four experiments. The IC₅₀ values are determined using GraphPad Prism (v7.03 for Windows, La Jolla, CA, USA), fitting the viability data to a sigmoidal curve mathematical model.

2.8. Fabrication of Alexa488-Labeled dsDNA-Loaded or GFP-DS RNA-Loaded PEG-PEI-PSilQ(cur) and PEI-PSilQ(cur) NPs. To prepare the Alexa488-labeled dsDNA or GFP-DS RNAloaded PEG-PEI-PSilQ(cur) or PEI-PSilQ(cur) materials, a molar ratio of amines/phosphates (N/P) of 10 was used.³⁴ Fluorescently labeled dsDNAs were used because of their cost benefits when compared to labeled dsRNA analogs. For loading of Alexa488-labeled dsDNA to the NPs, 1 mg of PEG-PEI-PSilQ(cur) or PEI-PSilQ(cur) NPs was suspended in 2 mL of the assembly buffer (pH = 8.2; 2 mM Ca^{2+} , Mg^{2+}). To this, Alexa488-labeled dsDNA (35 μ L of 10 μ M stock solution for N/P = 10) was added dropwise at room temperature. The final material was fabricated by incubating the dispersion for 30-45 min at 4 °C. The formed Alexa488-labeled dsDNA-loaded PEG-PEI-PSilQ(cur) or PEI-PSilQ(cur) NPs were centrifuged, washed, and redispersed in the assembly buffer to a final concentration of 1 mg/mL. The same protocol was used for the loading of GFP-DS RNA. Briefly, 1 mg of PEG-PEI-PSilQ(cur) or PEI-PSilQ(cur) was dispersed in 2 mL of assembly buffer. To this, 35 μ L of GFP-siRNA (N/P = 10) was added dropwise, and this was incubated for 30-45 min at 4 °C, resulting in formation of GFP-DS

RNA-loaded PEG-PEI-PSilQ(cur) or PEI-PSilQ(cur) NPs. The final material was centrifuged, washed, and redispersed in the assembly buffer to a final concentration of 1 mg/mL.

2.9. Evaluation of Cellular Uptake of Alexa488-Labeled dsDNA-Loaded PEG-PEI-PSilQ(cur) and PEI-PSilQ(cur) Nanoparticles. Flow cytometry and confocal laser scanning microscopy were used to evaluate the uptake of the Alexa488-labeled dsDNAloaded PEG-PEI-PSilQ NPs in MDA-MB-231 cells. For flow cytometry, MDA-MB-231 cells were cultured in a 24-well plate at a density of 2×10^4 cells per well in 0.5 mL of medium and incubated for 24 h at 37 °C and 5% CO₂ atmosphere. A volume of 0.5 mL of Alexa488-labeled dsDNA-loaded PEG-PEI-PSilQ(cur) or PEI-PSilQ-(cur) NPs was added to the cultured cells at a concentration of 30 μ g/ mL and incubated for 48 h. Afterward, the cells were washed, trypsinized, and collected for analysis in a flow cytometer (BD LSRFortessa cell analyzer) using mean FL-1 (green channel) and FL-2 (red channel) for Alexa488 and PpIX fluorescence, respectively. Free Alexa488-labeled dsDNA was also evaluated as the control sample. The results are reported as the average \pm SD of three independent experiments with two replicates each.

For confocal laser scanning microscopy, the MDA-MB-231 cells were seeded on a coverslip placed in six-well plates at a density of 5 × 10⁴ cells per well in 2 mL of DMEM and incubated at 37 °C in 5% CO₂ atmosphere for 24 h. After removing the culture medium, the cells were incubated with Alexa488-labeled dsDNA-loaded PEG-PEI-PSilQ(cur) and PEI-PSilQ(cur) NPs at a dose of 30 µg/mL in 2 mL of complete media for 48 h. Then, cells were washed three times with cold phosphate buffer solution. The cell nuclei were stained with Hoechst 33342 for 15 min. All microscopy images were acquired with an Olympus FluoView FV 1000 confocal laser scanning microscope.

2.10. Silencing of Green Fluorescent Protein Using Green Fluorescent Protein (GFP)-DS RNA-Loaded PEG-PEI-PSilQ(cur) and PEI-PSilQ(cur) NPs in MDA-MB-231/GFP Cells. The cell line MDA-MB-231/GFP stably expressing green fluorescent protein (the GFP gene was introduced using a lentivirus) was purchased from Cell Biolabs, Inc. For analysis with flow cytometry, MDA-MB-231/GFP cells were grown in 12-well plates at a concentration of 2×10^4 cells per well for 24 h. The cells were then exposed to different concentrations of GFP-DS RNA-loaded PEG-PEI-PSilQ(cur) and PEI-PSilQ(cur) materials (60, 100, and 150 $\mu g/mL$) and incubated for 48 h at 37 °C in 5% CO₂ atmosphere. Next, the cells were washed twice with phosphate buffer solution and incubated for an additional 24 h in fresh medium. After the incubation time, the cells were washed twice with phosphate buffer solution to remove particles that were not taken up. Cell dissociation buffer (100 μ L) was added to detach the cells from the culture plate. The cell suspension from each well was collected in separate tubes and gently shaken before analysis. The level of expression of GFP was determined by fluorescenceactivated cell sorting analysis on a FACSCalibur flow cytometer (BD Biosciences). At least 15,000 events were collected and analyzed using the CellQuest software. The data is reported in terms of the percentage of GFP silencing. The results are reported as the average \pm SD of three independent experiments.

For microscopy analysis, MDA-MB-231/GFP cells were seeded in a 24-well plate at a density of 1×10^4 cells per well in 0.5 mL of complete medium and incubated for 24 h at 37 °C in 5% CO₂ atmosphere. The cells were then exposed to three different concentrations of GFP-DS RNA-loaded PEG-PEI-PSilQ(cur) and PEI-PSilQ(cur) NPs (60, 100, and 150 μ g/mL) and incubated for 48 h at 37 °C in 5% CO₂ atmosphere. Next, the cells were washed twice with phosphate buffer solution and incubated for an additional 24 h in fresh medium. Finally, the plates were imaged to assess the GFP expression using the EVOS FL Imaging System (inverted four-color imaging system).

2.11. Influence of the Photochemical Internalization Effect on the Transfection of GFP-DS RNA in MDA-MB-231/GFP Cells. To assess the effect of photochemical internalization on the transfection efficacy of PEG-PEI-PSilQ and PEI-PSilQ NPs, MDA-MB-231/GFP cells were grown in 12-well plates at a concentration of 2×10^4 cells per well and incubated for 24 h at 37 °C in 5% CO₂

atmosphere. The cells were then exposed to three different concentrations of GFP-DS RNA-loaded PEG-PEI-PSilQ(cur) and PEI-PSilQ(cur) NPs (60, 100, and 150 $\mu \rm g/mL)$ and incubated for 48 h at 37 °C in 5% CO $_2$ atmosphere. Next, the cells were washed twice with phosphate buffer solution, subjected to light irradiation at a fluence rate of 24.5 mW/cm 2 for 5 min, and incubated for an additional 24 h in fresh medium. After the incubation time, the cells were washed with phosphate buffer solution twice to remove particles that were not taken up. Cell dissociation buffer was added (100 $\mu \rm L)$ to detach the cells from the culture plate. The cell suspension from each well was collected in separate tubes and gently shaken before analysis. The data is reported in terms of percentage of GFP silencing. The results are reported as the average \pm SD of three independent experiments.

2.12. Statistical Analysis. In this work, the phototherapeutic effect, ROS generation, uptake of nanoparticles, and transfection efficiency were analyzed by either one- or two-way univariate analysis of variance (ANOVA) model with the Bonferroni post hoc test. A value of p < 0.05 was considered statistically significant. Statistical analyses were performed by using GraphPad Prism (v7.03 for Windows, La Jolla, CA, USA).

3. RESULTS AND DISCUSSION

3.1. Synthesis of Redox-Responsive PpIX Silica Derivative 5. The synthesis of the redox-responsive PpIX silane ligand was performed through a series of sequential reactions, as shown in Scheme S1. First, the carboxylic acid groups in the PpIX molecule were activated using N-hydroxy succinimide through a coupling reaction mediated by a 1-ethyl-3-(3'-dimethylaminopropyl)carbodiimide intermediate to afford the PpIX derivative 2. Compound 2 reacted with cysteine hydrochloride in the presence of diisopropylethylamine, yielding molecule 3. Cysteine was used to produce the redox-responsive PSilQ platform. The thiol group in compound 3 was activated through a disulfide exchange reaction with dipyridine disulfide to afford 4. The final reaction between compound 4 and 3-mercaptopropyl triethoxysilane was carried out through another disulfide exchange reaction to produce the final redox-responsive PpIX silane ligand 5. Compounds 2-5 were characterized using spectroscopic techniques, as depicted in the Supporting Information.

3.2. Synthesis of PSilQ, PSilQ(cur), PEI-PSilQ(cur), and PEG-PEI-PSilQ(cur) Nanoparticles. The synthesis of PSilO NPs was performed by using the microemulsion method.³ This approach relies on the preferred distribution of a hydrophobic ligand into the oil droplet of the oil-in-water microemulsion. The use of microemulsions as nanoreactors has proven to be an effective method to reduce the polydispersity in the nanoparticle size. In addition, the hydrophobic nature of the nanodroplet can be used to solubilize and encapsulate a wide spectrum of hydrophobic drugs. In this work, we used dioctyl sulfosuccinate sodium salt as the surfactant, n-butanol as the cosurfactant, cyclohexane as the oil phase, and water as the continuous phase of the microemulsion system. Aqueous ammonia and NaOH solutions were added to enhance the solubility and accelerate the condensation of the PpIX silane precursor 5 (Scheme S2). By using this synthetic approach, PSilQ NPs with narrow size distribution and high loading of PpIX molecules were obtained (Figure 1 and Table 1). Moreover, we co-encapsulated curcumin inside PSilQ NPs as a model drug (PSilQ(cur) NPs). Curcumin is a well-known naturally occurring plantderived compound that is extracted from the Indian spice turmeric. 36 Several studies have confirmed the anticancer effect of curcumin against different types of cancer such as breast

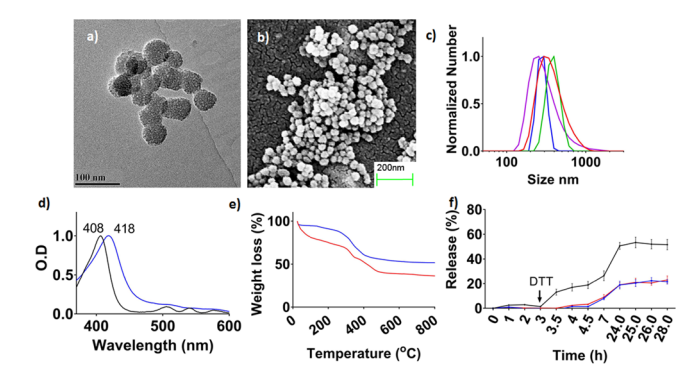


Figure 1. (a) TEM image of PSilQ NPs (diameter = 40 ± 5 nm; n = 50). (b) SEM image of PSilQ NPs. (c) DLS plot for PSilQ (blue), PSilQ(cur) (red), PEI-PSilQ(cur) (green), and PEG-PEI-PSilQ(cur) (purple) NPs. (d) Normalized UV—vis spectra of PpIX molecule (black) and PSilQ NPs (blue) in dimethyl formamide. (e) TGA plot for PSilQ (blue) and PSilQ(cur) NPs (red). (f) Release profile of PpIX in the presence of dithiothreitol at 10 mM (black) and 10 μ M (red) concentrations and in the absence of the reducing agent (blue). The release profile was carried out at 37 °C. The plot shows the average \pm SD of three independent experiments.

Table 1. Structural Properties of PSilQ Materials

material	DLS size (d, nm) (n = 5)	ζ -potential (mV) $(n = 5)$
PSilQ NPs	225 ± 25	-35 ± 3
PSilQ(cur) NPs	229 ± 45	-38 ± 2
PEI-PSilQ(cur) NPs	314 ± 18	$+10 \pm 1$
PEG-PEI-PSilQ(cur) NPs	271 ± 20	$+7.0 \pm 0$

cancer, cervical cancer, ovarian cancer, pancreatic cancer, prostate cancer, and neuroblastoma. $^{37-40}$

To further functionalize the PSilQ(cur) NPs, we took advantage of the negative charge produced by the carboxylate groups on the surface the PSilQ(cur) NPs, which are made available after the deprotonation of the carboxylic acids in compound 5 under physiological pH. The nanoparticles were modified through the electrostatic interaction with the positively charged polyethyleneimine (PEI, MW = 10 kDa) polymer to afford PEI-PSilQ(cur) NPs (Scheme 1 and Scheme S2). This modification allows the PEI-PSilQ(cur) platform to be used as a gene carrier by using the electrostatic binding of the cationic PEI polymer with the negatively charged dsDNA or RNA.41,42 Finally, the PEI-PSilQ(cur) NPs were further modified with polyethylene glycol (PEG, MW = 2 kDa) using coupling chemistry, as described in the Supporting Information, to fabricate PEG-PEI-PSilQ(cur) NPs. PEG molecules enhance the biocompatibility of nanoparticles and circulation time in vivo. 43,44

3.3. Characterization of PSilQ, PSilQ(cur), PEI-PSilQ(cur), and PEG-PEI-PSilQ(cur) Nanoparticles. The physicochemical properties of the different PSilQ materials were characterized using transmission electron and scanning electron microscopy (TEM and SEM, respectively), dynamic light scattering (DLS), ζ -potential, UV-vis and fluorescence spectroscopy, thermogravimetric analysis (TGA), Kaiser's assay, ultrahigh-performance liquid chromatography (UHPLC), and ${}^{1}O_{2}$ generation. TEM and SEM were used to analyze the particle size and morphology of the fabricated PSilQ NPs. The nanoparticles are spherical in shape with an average diameter of 40 ± 5 nm (n = 50 particles), as depicted

in Figure 1a,b. The hydrodynamic diameter and ζ -potential of the different PSilQ materials were characterized by DLS and the electrophoretic mobility in phosphate buffer solution (1 mM) (Figure 1c and Table 1), respectively. The PSilQ NPs showed a hydrodynamic diameter of 255 ± 25 nm, which is larger than the physical diameter measured by TEM and SEM. Aggregation of the nanoparticles in phosphate buffer solution and swelling caused by the hydration of the silica network of the PSilQ NPs may account for this observation. 45,46 A negative value of -35 ± 3 mV for the ζ -potential was measured, which is indicative of the presence of carboxylate groups on the surface of the PSilQ NPs (Table 1). The coencapsulation of curcumin to afford PSilQ(cur) NPs had a negligible effect on the hydrodynamic diameter and ζ -potential of the nanoparticles (229 \pm 40 nm and -38 ± 2 mV, respectively). Nevertheless, after surface modification of the PSilQ(cur) NPs with a PEI polymer, both the hydrodynamic diameter and ζ -potential increased from 229 \pm 40 to 314 \pm 18 nm and from -38 ± 2 to $+10 \pm 1$ mV, respectively. The increase in aggregation is due to the reduction in electrostatic repulsion but is also indicative of the successful coating of PSilQ(cur) NPs with a PEI polymer. Further functionalization of the PEI-PSilQ(cur) NPs with a PEG polymer reduced the hydrodynamic diameter but without much variation in the ζ potential (271 \pm 20 nm and + 7 mV, respectively). The steric effect due to the PEG chains increased the repulsion between nanoparticles in dispersion, which resulted in the decrease in the hydrodynamic diameter.

To study the colloidal stability of the PSilQ platform, PEG-PEI-PSilQ(cur) and PSilQ(cur) NPs were redispersed in cell media containing fetal bovine serum. The hydrodynamic diameter of these dispersions was measured over a period of 15 h. There is a reduction of \sim 125 and \sim 60 nm on the initial hydrodynamic diameter value for PEG-PEI-PSilQ(cur) and PSilQ(cur) NPs compared with the one observed in phosphate buffer solution. Because of the interaction of the nanoparticles with serum, it was observed that both nanomaterials are colloidally stable in cell culture media supplemented with fetal bovine serum over a period of 15 h (Figure S1).

The UV-vis spectrum of free PpIX and PSilQ NPs in dimethyl formamide showed the characteristic Soret and Q bands for porphyrin molecules (Figure 1d). A red shift from 408 to 418 nm for the Soret band of the PSilQ NPs was observed when compared with free PpIX. This effect can be explained by the close packing of the PpIX molecules in the framework of the PSilQ platform, which results in a bathochromic shift typical of J-aggregates for porphyrins as has been reported for other nanoparticles. 13,47 The fluorescence spectra of free PpIX and PSilQ NPs revealed a sevenfold decrease in the fluorescence intensity for the nanoparticle formulation in comparison with free PpIX (Figure S2). The decrease in fluorescence intensity is accounted by the self-quenching effect due to the close proximity and strong intermolecular forces between hydrophobic PpIX molecules in this type of nanoparticulate system. This observation has also been reported in other polymeric systems and PSilQ platforms containing porphyrins. 13,44

Thermogravimetric analysis and UV-vis spectroscopy were used to determine the amount of PpIX loaded to the PSilQ NPs. TGA showed a loss in total organic content in three batches in the range of 46–52%, which correspond to 24.4 \pm 2.5 wt % of PpIX (450 \pm 50 μ mol/g; n = 3) (Figure 1e and Table S1). The PpIX loading was further corroborated by

UV-vis spectroscopy by measuring the absorbance of PpIX in PSilQ NPs in dimethyl formamide (25.8 \pm 10.0 wt %; n = 3).

To quantify the amount of primary amines chemically available on the surface of the PSilQ NPs after functionalization with a PEI polymer, the ninhydrin-based Kaiser's test was performed.³¹ The amounts of chemically accessible primary amines obtained for PEG-PEI-PSilQ(cur) and PEI-PSilQ(cur) NPs were 328 \pm 10 and 536 \pm 45 nmol per mg of nanoparticles (n = 3), respectively (Table S1).

The loading of curcumin into PSilQ(cur) NPs was determined indirectly by analyzing the amount of curcumin left in the supernatant after particle synthesis.⁴⁹ Curcumin concentration was calculated using UHPLC. The analysis showed negligible amount of curcumin present in the supernatant, ~1.0 wt % of the total amount of curcumin added, as an indication that the other 99.0 wt % of the curcumin was incorporated into the PSilQ(cur) NPs (201.5 nmol/mg; 7.6 ± 1.5 wt %). Furthermore, TGA (Figure 1e) showed an increase of 8.5 ± 1.5 wt % in the percentage of organic content for PSilQ(cur) NPs compared to PSilQ NPs. This data additionally confirms the loading of curcumin obtained by UHPLC.

The stability of the PEG-PEI-PSilQ(cur) and PEI-PSilQ-(cur) NPs under physiological and acidic conditions was determined indirectly by measuring the amount of primary amines associated to the PEI on the surface of the nanoparticles after different times of incubation (24 and 48 h). Figure S3 shows the results for the three different pH levels tested in this experiment: pH 7.4, 6.2, and 5.5. No statistically significant difference was observed in the amount of amine groups on the surface of the nanoparticles for the PEG-PEI-PSilQ(cur) or PEI-PSilQ(cur) materials at different pH levels even after 48 h of incubation (two-way ANOVA, p > 0.9). These results demonstrate that both PEG-PEI-PSilQ(cur) and PEI-PSilQ(cur) NPs are stable under physiological and acidic conditions.

3.4. Triggered Release via Reductive Environment. Recently, efforts have been made for the development of stimuli-responsive delivery systems. ^{50,51} We have shown in previous reports that by using a disulfide bond as part of the building unit for the fabrication of porphyrin-based PSilQ NPs, redox-responsive properties can be observed in the degradation of the platform. 10,115 Some advantages have been demonstrated by using this approach: (1) the presence of the disulfide bond can further enhance the degradable properties of the PSilQ platform, 52 and (2) there is an "off/on" effect that provides higher specificity at the targeted tumor tissue. 48 The "off" state is due to the self-quenching effect associated to the closed proximity of the photosensitizers encapsulated in the PSilQ NPs that reduce the generation of ¹O₂. The "on" state is related to the degradation of the PSilQ NPs after internalization by cancer cells due to the reducing environment, thus releasing photosensitizers as individual molecules, which efficiently generate ¹O₂ (Scheme S3). In this work, the controlled release of PpIX under a high reducing environment was investigated. The reducing agent concentrations of 10 μM and 10 mM were selected for this study because those are typical concentrations found in extracellular (2-20 μ M) and intracellular (2–10 mM) conditions. 25,53 As depicted in Figure 1f, there is minimal leakage of PpIX from the PSilQ NPs before the addition of the reducing agent dithiothreitol. However, a burst release of ~10-15% PpIX was observed immediately after the addition of the reducing agent (10 mM). This is

attributed to the cleavage of the disulfide bond on the surface of the PSilQ NPs. A plateau was reached at about 24 h. The amount of PpIX released from the PSilQ NPs in the presence of dithiothreitol was ~50% of the amount originally loaded to the NPs. For the experiments using 10 µM dithiothreitol and without dithiothreitol, ~20% of PpIX was released over 24 h. The release of PpIX observed for these samples could be attributed to the hydrolysis of the silica bond.⁵⁴ Overall, the results demonstrate that the presence of dithiothreitol at a concentration of 10 mM triggers the reduction of disulfide bonds within the PSilQ NPs framework, resulting in the selective release of PpIX molecules.

3.5. Photostability and ¹O₂ Generation Studies in Solution. Photobleaching is one of the most frequent drawbacks for the long-term use of photosensitizers. 35 It occurs due to the degradation and loss of fluorescence intensity of the PS molecule under light conditions. To evaluate the photostability of the NPs, PSilQ and PSilQ(cur) NPs were exposed to red light (630 nm) at a fluence rate of 24.5 mW/cm² for 20 min. Free PpIX at the same concentration of the one loaded into the nanoparticles was used as the control. There is a 20% decrease in fluorescence intensity for both nanomaterials after irradiation with red light (Figure S4). However, there is a greater reduction of more than 60% in the fluorescence of PpIX molecules as an indication of photobleaching. Photodegradation is mainly associated with the chemical decomposition of the photosensitizer molecules in the presence of ROS. 55 We hypothesize that the "off" state of the PSilQ and PSilQ(cur) NPs due to the self-quenching effect is the primary cause for the improved photostability of the nanoparticles in comparison with free PpIX molecules.

The production of reactive oxygen species is usually associated with the phototoxic effect; nevertheless, for photodynamic therapy, the generation of singlet oxygen (1O2) molecules is essential for producing a phototoxic effect. 56 We have shown that despite the "off" state of the porphyrins localized in the framework of the PSilQ NPs, generation of ¹O₂ still occurs due to the molecules on the surface of the nanoparticles. 15 To verify the ability of PSilQ and PSilQ(cur) NPs to produce ¹O₂, 9,10-anthracene dipropionic acid, a singlet oxygen probe, was used. The absorbance of this singlet oxygen probe at 378 nm was monitored in the presence of each nanoparticle after light exposure (630 nm; fluence rate, 24.5 mW/cm²) at different irradiation times (0, 5, 10, 15, and 20 min). As shown in Figure S5, the absorption intensity of 9,10-anthracene dipropionic acid at 378 nm decreased gradually as a function of irradiation time, indicating that ¹O₂ molecules are produced by both PSilQ and PSilQ(cur) NPs. Control experiments in the absence of light did not show a significant change in the absorption intensity of the singlet oxygen probe at 378 nm.

3.6. Phototherapy and Chemotherapy Using the PSilQ and PSilQ(cur) Platform To Treat MDA-MB-231 Cells. Photodynamic therapy (PDT) is a localized therapeutic approach for potential eradication of malignant tissues. PDT has been used to treat different types of cancer such as skin cancer, head and neck cancer, and lung cancer in clinical settings.⁵⁸ Recently, the first clinical trial to treat breast cancer with PDT was performed (NCT02872064). In particular, the treatment of TNBC is presenting major challenges, requiring the implementation of multimodal strategies to obtain improved outcomes. 19,20 The use of PDT in combination with other therapies such as chemotherapy and/or gene therapy can be very impactful in treating TNBC. The phototoxicity and cytotoxicity of PSilQ materials in MDA-MB-231 cells were evaluated using the MTS assay (Figure 2

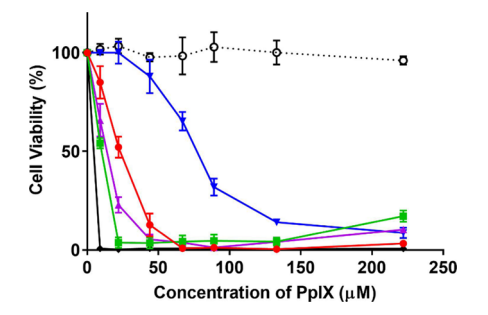


Figure 2. Combined phototoxicity and cytotoxicity of PpIX (black), silica nanoparticles (dotted line), PSilQ NPs (blue), PSilQ(cur) NPs (red), PEI-PSilQ(cur) NPs (green), and PEG-PEI-PSilQ(cur) NPs (purple) against MDA-MB-231 cells. The amount of curcumin for each experimental point is reported in Table S2. Incubation time was 48 h, followed by irradiation at 24.5 mW/cm² for 20 min. Data points show the average and SD of four experiments.

Table 2. IC₅₀ Values for Combined Phototoxicity and Cytotoxicity of PpIX, Curcumin, and PSilQ Materials in MDA-MB-231 Cells

	$IC_{50} (PpIX/\mu M)$		IC ₅₀ (curcumin/μM)	
material	light	dark	light	dark
PpIX	4.9	46.4	NA	NA
curcumin	NA	NA	49.1 ^b	54.7 ^b
PSilQ NPS	76.7	91.6	NA	NA
PSilQ(cur) NPs	21.7	170.0	9.9	78.2
PEI-PSilQ(cur) NPs	9.3	94.1	4.3	43.3
PEG-PEI-PSilQ(cur) NPs	12.2	115.3	5.1	53.0

^aNA, not applicable. ^bIndicates no statistical difference between values (one-way ANOVA, p > 0.5).

and Table 2). PSilQ NPs showed a dose-dependent phototoxicity against MDA-MB-231 cells upon light irradiation at 24.5 mW/cm² for 20 min with an IC₅₀ value of 76.7 μ M. In the case of PSilQ(cur) NPs, there was a 3.5-fold reduction in the IC_{50} for PpIX ($IC_{50} = 21.7 \mu M$) compared to PSilQ NPs under the same irradiation conditions. Curcumin has been recently used as a photosensitizer when irradiated with blue light.⁵⁹ However, as shown in Figure S6, curcumin induced a similar toxic effect under dark and red light (630 nm) conditions toward MDA-MB-231 cells (IC₅₀ = 58.5 μ M). The lack of absorbance in the red region for the molecule of curcumin can explain the absence of phototoxicity. 60 The IC₅₀ value of PSilQ(cur) NPs based on the curcumin was 9.9 μ M, which is five times lower than that for free curcumin. These results showed a synergistic effect between curcumin and PpIX. The anticancer activity of curcumin is associated to the regulation of multiple signaling pathways.²⁶ Particularly for TNBC cells, NF- κ B, PI3K/Akt, and TGF- β pathways are some of the main targets for curcumin.²⁸ The mechanisms and signaling pathways that are involved in the combinatorial effect of PpIX and curcumin against MDA-MB-231 cells have yet to be investigated. Bare silica nanoparticles were used as a control material to rule out any possibility of phototoxicity due to

silica. After light irradiation at 24.5 mW/cm² for 20 min, there was no reduction in the viability of MDA-MB-231 cells.

The combined phototoxicity and cytotoxicity of the PSilQ(cur) NPs after modification with PEI and PEG polymers were also determined. Cell survival analysis showed that PEI- and PEG-functionalized materials have slightly higher toxicity than PSilQ(cur) NPs based on PpIX (IC₅₀ = 9.3 and 12.2 μ M, respectively) and curcumin content (IC₅₀ = 4.3 and 5.1 μ M, respectively) (Figure 2 and Table 2). This increase in cell death efficiency can be attributed to the cationic surface of PEG-PEI-PSilQ(cur) and PEI-PSilQ(cur) NPs, which render higher cellular internalization than PSilQ(cur) NPs.

In dark conditions, PpIX encapsulated into the PSilQ NPs is less cytotoxic than free PpIX (IC₅₀ = 46.4 μ M vs 91.6 μ M) (Figure S7 and Table 2). In the case of the PSilQ(cur) NPs, the cytotoxicity of PpIX is reduced even further compared to that of free PpIX ($\overline{IC}_{50} = 170.0 \mu M$). This effect has been observed before, and it is most likely due to the antioxidant properties of curcumin. 61 The cytotoxicity of curcumin encapsulated in PSilQ(cur) NPs is slightly lower than that of free curcumin (IC₅₀ = 78.2.4 μM vs 54.7 μM). As shown in Figure S7 and Table 2, PEI coating increased the cytotoxicity of the NPs for PpIX (IC₅₀ = 94.1 μ M) due to the high density of positive charges from PEI, but further functionalization with PEG polymer reduced the toxic effect (IC₅₀ = 115.3 μ M). The cytotoxicity of curcumin encapsulated in PEG-PEI-PSilQ(cur) and PEI-PSilQ(cur) NPs (IC₅₀ = 43.3 and 53.0 μ M, respectively) is similar to the one observed for free curcumin $(IC_{50} = 54.7 \ \mu M).$

Similarly, the importance of having a therapeutic effect in TNBC cells is to avoid toxicity in normal breast cells. To assess the combined phototoxicity and cytotoxicity of the NPs against healthy cells, normal human epithelial cell line MCF-10A was incubated with PSilQ(cur) NPs and treated under the same conditions as was used for MDA-MB-231 cells. Both the phototoxicity and dark toxicity of free PpIX are at least 100fold higher than those observed for PpIX encapsulated in PSilQ(cur) NPs (Figure S8 and Table S3). These differences are due to the mechanisms that either free PpIX or PSilQ(cur) NPs use for internalization in mammalian cells. PpIX, the main component of heme, is usually internalized by protein transporters, 62 while NPs usually undergo endocytosis for cellular uptake.

3.7. Measurement of Intracellular Reactive Oxygen Species Generated by PSilQ and PSilQ(cur) Nanoparticles. The generation of reactive oxygen species is a critical factor in producing the phototoxic effect of PS molecules against cancer cells. To investigate the intracellular production of ¹O₂ by PSilQ or PSilQ(cur) NPs, we utilized an indirect method using the singlet oxygen sensor green (SOSG) probe.⁶³ SOSG is a cell-impermeable compound, highly selective for ¹O₂, which is used to quantify ¹O₂ ⁶⁴ This ¹O₂ probe emits strong green fluorescence after reacting with ¹O₂. Lysed samples of MDA-MB-231 cells incubated with different concentrations of PSilQ or PSilQ(cur) NPs were irradiated with red light (630 nm) at 24 mW/cm² for 20 min in the presence of the ¹O₂ probe. The production of ¹O₂ is concentration-dependent as seen in Figure 3a, which corresponds to the amount of PpIX carried by the PSilQ or PSilQ(cur) NPs. There is no statistical difference for ¹O₂ generation for either the PSilQ or PSilQ(cur) NPs at any of the concentrations evaluated in this work (two-way ANOVA, p > 0.5). This result corroborates that curcumin encapsulated in

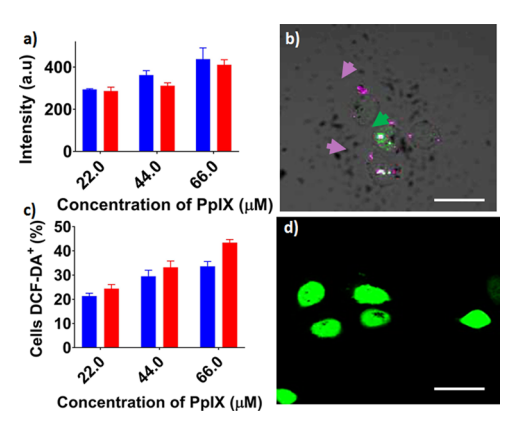


Figure 3. (a) Singlet oxygen quantification using SOSG for PSilQ (blue) and PSilQ(cur) (red) NPs at three different concentrations of PpIX (22.0, 44.0, and 66.0 μ M) after red light irradiation (630 nm, 24 mW/cm² for 20 min). (b) Confocal micrograph of MDA-MB-231 cells inoculated with SOSG-loaded PSilQ(cur) NPs. Arrows indicate the fluorescence of NPs (purple) and SOSG (green) after light irradiation. (c) In vitro detection of ROS using the DCFH-DA probe. MDA-MB-231 cells were inoculated with PSilQ (blue) and PSilQ(cur) (red) NPs and irradiated with red light (630 nm, 24 mW/cm² for 20 min). The ROS-positive MDA-MB-231 cells were quantified using flow cytometry. (d) Confocal image of MDA-MB-231 cells treated with PSilQ(cur) NPs and red light in the presence of the DCFH-DA probe. The strong green fluorescence depicts the generation of ROS. Data points in (a) and (c) show the average and SD of three independent experiments. Statistical analysis was performed by two-way ANOVA; no statistical difference was found (p > 0.5). Scale bar, 30 μ m.

the framework of the PSilQ(cur) NPs does not have a major impact on the formation of ${}^{1}O_{2}$. Control experiments were carried out with MDA-MB-231 cells incubated in the presence of PSilQ and PSilQ(cur) NPs under dark conditions (Figure S9). In all experiments, minimal increase in fluorescence was observed, suggesting that the PSilQ NPs under light irradiation are mainly responsible for the generation of ¹O₂.

Singlet oxygen sensor green (SOSG) molecules were passively loaded to the PSilQ(cur) NPs to further prove that PSilQ(cur) NPs can generate ¹O₂ inside MDA-MB-231 cells. This strategy has been used with other nanocarriers and has the advantage of allowing the cell membrane-impermeable SOSG molecule to be transported inside the cells.⁶³ Figure 3b shows a merged confocal image for cells incubated with SOSGloaded PSilQ(cur) NPs after irradiation with red light. Green fluorescence from the 1O2 probe was observed inside the MDA-MB-231 cells as an illustration showing that the SOSG molecules were transported through the cell membrane and able to detect the generation of ¹O₂. The control experiment, where MDA-MB-231 cells are treated with the PSilQ(cur) NPs followed by incubation with the ¹O₂ probe, did not show green fluorescence inside the cells (Figure S10). The peripheral fluorescence observed in the micrograph can be attributed to generated 1O2 molecules that diffused out across the cell membrane and reacted with the 1O2 probe that was physisorbed on the membrane.

The ability of PSilQ and PSilQ(cur) NPs to produce other reactive oxygen species in MDA-MB-231 cells was characterized using 2',7'-dichlorodihydrofluorescein diacetate (DCFH-DA), an ROS probe. 65 Once inside the cells, the diacetate group of DCFH-DA is removed by intracellular esterases. The remaining molecule is then oxidized by ROS to produce 2',7'-dichlorofluorescein, which emits green fluorescence.³² In this work, the cells were incubated with different concentrations of nanoparticles and irradiated using red light (630 nm, 24.5 mW/cm²) for 20 min. The positive cells showing the green fluorescence produced by the oxidation of DCFH-DA with ROS were quantified using flow cytometry. The production of ROS for both nanomaterials PSilQ and PSilO(cur) NPs is concentration-dependent (Figure 3c). There is no statistical significant difference between the amount of reactive oxygen species generated by PSilQ and PSilQ(cur) NPs (two-way ANOVA, p > 0.5). Confocal micrographs showed strong green fluorescence in MDA-MB-231 cells incubated with PSilQ NPs after light irradiation, confirming the generation of ROS (Figure 3d). Control experiments in the absence of light and nanoparticles depicted a reduction of green fluorescence inside the MDA-MB-231 cells, presumably due to the presence of endogenous ROS (Figure S11). The results from these experiments confirmed that PSilQ and PSilQ(cur) NPs can efficiently transport PpIX molecules inside the MDA-MB-231 cells and generate reactive oxygen species, which are critical elements for the efficacy of PDT. Moreover, the data also supports the fact that curcumin is not a major player in the production of reactive oxygen species under the conditions used for our experiments.

3.8. PSilQ(cur) Platform as Efficient Carrier for the Intracellular Transport of Nucleic Acids. The multifunctional capabilities of the PSilO(cur) platform to carry the genetic material were tested in vitro using the PEG-PEI-PSilQ(cur) and PEI-PSilQ(cur) NPs. First, to study the transport and internalization of genetic material, Alexa488labeled dsDNA was loaded to both PEG-PEI-PSilQ(cur) and PEI-PSilQ(cur) NPs. MDA-MB-231 cells were incubated with these materials (30 μ g/mL) for 48 h. Flow cytometry showed that the nanoparticles were internalized (Figure 4a) and efficiently carried Alexa488-labeled dsDNA into MDA-MB-231 cells in comparison with free Alexa488-labeled dsDNA (Figure 4b). No statistical differences (one-way ANOVA, p > 0.7) were found between PEG-PEI-PSilQ(cur) and PEI-PSilQ(cur) NPs for the cellular uptake of the nanoparticles nor Alexa488labeled dsDNA under the conditions used for the experiment. The cellular internalization of Alexa488-labeled dsDNA-loaded PEG-PEI-PSilQ(cur) and PEI-PSilQ(cur) NPs was further confirmed by confocal microscopy (Figure 4c-e). Both the green and red channels depicted the presence of Alexa488labeled dsDNA and PEG-PEI-PSilQ(cur) or PEI-PSilQ(cur) NPs, respectively (Figure 4c2-e2,c3-e3). The merged images confirmed that NPs successfully underwent cellular uptake by MDA-MB-231 cells and efficiently released Alexa488-labeled dsDNA in the cytoplasm (Figure 4d4,e4). Control experiments using only Alexa488-labeled dsDNA confirmed that the presence of PEG-PEI-PSilQ(cur) and PEI-PSilQ(cur) NPs is required for the successful transport of nucleic acids inside MDA-MB-231 cells (Figure 4c2,c3).

The combinatorial use of RNA interference (RNAi) inducers in this study was motivated by the recent approval of the first RNAi therapeutic agent (patisiran) by the FDA.²⁹ The GFP-DS RNAs used for green fluorescent protein silencing were designed to produce siRNAs upon cytosolic processing by Dicer and further activation of RNAi.³⁰ DS RNAs have been previously utilized in various nanoformulations, resulting in high levels of silencing efficiencies. 66-68 GFP-DS RNAs were used to further verify the delivery properties of PEG-PEI-PSilQ(cur) and PEI-PSilQ

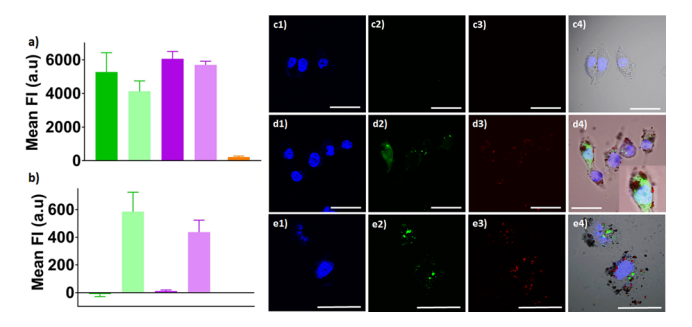


Figure 4. MDA-MB-231 cells uptake of Alexa488-labeled dsDNA and Alexa488-labeled dsDNA-loaded PEG-PEI-PSilQ(cur) and PEI-PSilQ(cur) NPs. (a) Mean red fluorescence intensity associated to PEG-PEI-PSilQ(cur) and PEI-PSilQ(cur) NPs obtained from flow cytometry experiments after inoculation with PEI-PSilQ(cur) (green), Alexa488-labeled dsDNA-loaded PEI-PSilQ(cur) (light green), PEG-PEI-PSilQ(cur) (purple), Alexa488-labeled dsDNA-loaded PEG-PEI-PSilQ(cur) (light purple) NPs, and Alexa488-labeled dsDNA (orange). (b) Mean green fluorescence intensity associated to Alexa488-labeled dsDNA obtained from flow cytometry experiments after inoculation with the same materials described in (a). Statistical analysis by one-way ANOVA showed no difference in the internalization for both (a) and (b) (p > 0.7). (c) Confocal micrographs of MDA-MB-231 cells inoculated with Alexa488-labeled dsDNA (c1c4), Alexa488-labeled dsDNA-loaded PEI-PSilQ(cur) (d1-d4), and Alexa488-labeled dsDNA-loaded PEG-PEI-PSilQ(cur) (e1-e4) NPs. The cell nuclei are observed in the blue channel after staining with Hoechst 33342 (c1, d1, e1). The fluorescence in the FITC (green) channel (c2, d2, e2) indicates the localization of Alexa488-labeled dsDNA. The fluorescence in the TRITC (red) channel shows the presence of PSilQ(cur) NPs (c3, d3, e3). The merged micrographs (c4, d4, e4) show the colocalization and localization of Alexa488labeled dsDNA and NPs inside MDA-MD-231 cells. The inset in (d4) clearly demonstrates the release of Alexa488-labeled dsDNA from PEI-PSilQ(cur) NPs. Scale bar, 40 μ m.

NPs. MDA-MB-231 cells expressing green fluorescent protein were used (MDA-MB-231/GFP). Different amounts of GFP-DS RNA were loaded to PEG-PEI-PSilO(cur) and PEI-PSilQ(cur) NPs to evaluate the silencing of green fluorescent protein. Table S4 shows the amount of loaded GFP-DS RNA per concentration of nanoparticles. PEI-PSilQ(cur) NPs showed a higher capacity of GFP-DS RNA loading than the PEGylated version with a maximum loading of 138 nM versus 84 nM at 150 μ g/mL. Control experiments using free GFP-DS RNA and Lipofectamine 2000 (L2K) were also performed. MDA-MB-231/GFP cells treated with the GFP-DS RNAloaded nanoparticles were analyzed by flow cytometry to determine the transfection efficiency of the PEG-PEI-PSilQ-(cur) and PEI-PSilQ(cur) NPs (Figure 5a). The flow cytometry data proved that silencing of green fluorescent protein is concentration-dependent but with the highest concentration of nanoparticles (150 μ g/mL) being statistically the most efficient (one-way ANOVA, p < 0.05 and p < 0.01). At this concentration, the efficiency values of GFP silencing were 40.3 ± 1.5 and $54.4 \pm 2.5\%$ for PEG-PEI-PSilQ(cur) and PEI-PSilQ(cur) NPs, respectively. Lipofectamine 2000 carrier was used for the positive control experiment with a GFP silencing efficiency of 63.1 ± 8.8%. Lipofectamine 2000 is statistically more efficient for GFP silencing in comparison with both nanoparticles at different concentrations (two-way ANOVA, p < 0.05-0.0001), with the exception of PEI-PSilQ(cur) NPs at 150 μ g/mL, which is statistically similar to Lipofectamine (two-way ANOVA, p > 0.7). Control experi**ACS Applied Materials & Interfaces**

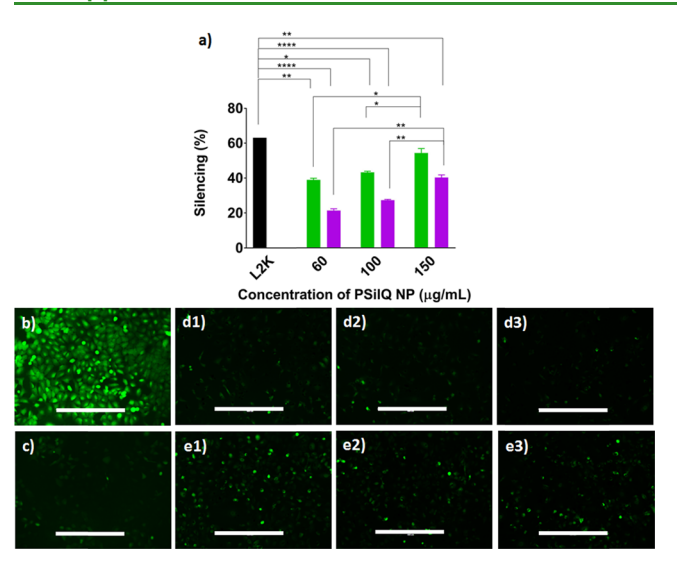


Figure 5. (a) GFP silencing efficiencies for GFP-DS RNA with L2K (control, black), PEI-PSilQ(cur) (green), and PEG-PEI-PSilQ(cur) (purple) NPs used as transfection vectors. Statistical analysis was performed by two-way ANOVA (*p < 0.05, **p < 0.01, ***p < 0.001, ***p < 0.0001) to analyze the differences in GFP silencing between L2K and the NPs at different concentrations. One-way ANOVA was used to determine the statistical difference in GFP silencing for each individual NP at different concentrations. Microscopy images of MDA-MB-231/GFP cells (b) before and (c) after GFP-DS RNA transfection with L2K or PEI-PSilQ(cur) NPs (d1-d3) or PEG-PEI-PSilQ(cur) NPs (e1-3). The following concentrations of NPs were used: 60 μ g/mL (d1, e1), 100 μ g/mL (d2, e2), and 150 μ g/mL (d3, e3). Scale bar, 400 μ m.

ments with free GFP-DS RNA showed 0% transfection. These results confirmed that GFP-DS RNA indeed needs an efficient carrier to be able to afford any transfection. The data demonstrated that PEG-PEI-PSilQ(cur) and PEI-PSilQ(cur) NPs are promising platforms to efficiently transport and deliver GFP-DS RNA inside MDA-MB-231/GFP cells. Fluorescence microscopy was further used to confirm the results obtained by flow cytometry (Figure 5b-e). Our negative and positive control experiments depicted a higher population of MDA-MB-231/GFP cells expressing green fluorescent protein, which is silenced after transfection of GFP-DS RNA with L2K (Figure 5b,c). The fluorescence micrographs clearly showed a dramatic reduction in the expression of green fluorescent protein after transfecting MDA-MB-231/GFP cells with GFP-DS RNA using PEG-PEI-PSilQ(cur) or PEI-PSilQ(cur) NPs as vectors at different concentrations (Figure 5d1-d3,e1-e3). A concentration-dependent trend can be observed in the GFP silencing, which was already quantitatively confirmed by flow

One of the main challenges for nanoparticle-based gene delivery systems is to escape from the endolysosomal pathway to efficiently deliver the genetic material in the cytoplasm.⁶⁹ One alternative that has attracted attention in recent years is the use of photosensitizers to enhance endolysosomal escape. Photoinduced generation of reactive oxygen species could disrupt the endolysosomal membranes to facilitate nanoparticle escape and enhance gene transfection; this effect has been called photochemical internalization.⁷⁰ In this work, by taking advantage of the multimodal capabilities of the PSilQ platform, we explore the photochemical internalization effect on the delivery of GFP-DS RNA.

MDA-MB-231/GFP cells were transfected with the GFP-DS RNA-loaded PEG-PEI-PSilQ(cur) and PEI-PSilQ(cur) NPs followed by irradiation with red light (630 nm) at a rate of 24.5 mW/cm² for 5 min. This light fluence does not produce a phototoxic effect but still allows the generation of reactive oxygen species. Similar to the transfection experiments in the absence of light, the silencing of green fluorescent protein is concentration-dependent with the PEI-PSilQ(cur) NPs at 100 and 150 µg/mL and statistically has been the most efficient method (one-way ANOVA, p < 0.05) (Figure S11). At these concentrations, the efficiency values of GFP silencing were 47.1 ± 2.5 and $61.0 \pm 0.3\%$. Both concentrations had statistically similar transfection efficiency to that of Lipofectamine (two-way ANOVA, p > 0.07 and p > 0.99, respectively). By comparing the GFP silencing in the absence and presence of light for both the PEG-PEI-PSilQ(cur) and PEI-PSilQ(cur) NPs at the same concentration, a clear trend is observed in the enhancement of GFP-DS RNA transfection in those experiments that have been irradiated with light (Figure S12), but the differences are not statistically significant other than PEG-PEI-PSilQ NPS at 60 μ g/mL (two-way ANOVA, p < 0.01). Nevertheless, these results confirmed that the photochemical internalization effect induced by the PEI-PSilQ(cur) platform can be a promising approach to enhance RNAi transfection. Because of the recent success of RNAi in the clinic, any further developments to enhance the therapeutic effect of this innovative technology become of great importance.

4. CONCLUSIONS

We have designed and fabricated a novel redox-responsive multimodal system based on the polysilsesquioxane nanoparticulate platform for the efficient delivery of PpIX, curcumin, and RNAi-inducing agent (GFP-DS RNA) in TNBC cells. The PSilQ(cur) NPs have high loading capacities for PpIX (24.4 \pm 2.5 wt %) and curcumin (7.6 \pm 1.5 wt %). This platform shows a synergistic effect for the phototherapy and chemotherapy treatment against the cell line MDA-MB-231. Interestingly, the PSilQ(cur) NPs are more selective to kill MDA-MB-231 cells compared to normal MCF-10A breast cells, which is relevant for future preclinical and clinical applications of this platform. The modified PEG-PEI-PSilQ-(cur) and PEI-PSilQ(cur) NPs efficiently carry and deliver DNA and RNAi inducers. The transfection efficiency of this platform is comparable to Lipofectamine 2000, which is the gold standard for transfection in vitro. By using the photochemical internalization approach, the transfection can be further enhanced. These results contribute to the establishment of the PSilQ nanoplatform that can serve multiple functions and is deemed useful in future experiments for its multimodality toward cancer therapeutics and other diseases.

ASSOCIATED CONTENT

Supporting Information

The Supporting Information is available free of charge on the ACS Publications website at DOI: 10.1021/acsami.9b00704.

> Materials and methods, synthetic procedures for compounds 2-5, physicochemical characterization of PSilQ NPs, and the details of cell culture protocols (PDF)

AUTHOR INFORMATION

Corresponding Author

*E-mail: jviveroe@uncc.edu.

ORCID ®

Ridhima Juneja: 0000-0002-1260-9652 Zachary Lyles: 0000-0001-5291-6545

Hemapriyadarshini Vadarevu: 0000-0003-3172-6579

Kirill A. Afonin: 0000-0002-6917-3183 Juan L. Vivero-Escoto: 0000-0001-7400-2963

Funding

J.L.V.-E. and K.A.A. received funding from the National Science Foundation (EAGER-NSF #1835688), SPRINT UNCC-FAPESP award, Faculty Research Grant award (FRG/UNC Charlotte), and the Department of Chemistry, UNC Charlotte start-up funds.

The authors declare no competing financial interest.

ACKNOWLEDGMENTS

We would like to thank graduate students Mubin Tarannum for the TEM micrographs and Justin Halman for the duplex preparations. We also would like to thank Dr. Vanderlei Bagnato (CePOF/INOF, University of São Paulo, Brazil) for generously providing the home-made LED device used to perform the in vitro phototoxic experiments. Curcumin was kindly supplied by Dr. Kleber Thiago de Oliveira (Federal University of São Carlos, Brazil). We also thank Jessica McMillan for the critical reading.

REFERENCES

- (1) Kim, D.; Shin, K.; Kwon, S. G.; Hyeon, T. Synthesis and Biomedical Applications of Multifunctional Nanoparticles. Adv. Mater. **2018**, *30*, 1802309.
- (2) Hayashi, K. Multifunctional Silica-Based Hybrid Nanoparticles for Biomedical Applications. J. Ceram. Soc. Jpn. 2016, 124, 855-862.
- (3) Baeza, A.; Ruiz-Molina, D.; Vallet-Regí, M. Recent Advances in Porous Nanoparticles for Drug Delivery in Antitumoral Applications: Inorganic Nanoparticles and Nanoscale Metal-Organic Frameworks. Expert Opin. Drug Deliv. 2017, 14, 783-796.
- (4) Lin, W.; Rieter, W. J.; Taylor, K. M. L. Modular Synthesis of Functional Nanoscale Coordination Polymers. Angew. Chem., Int.Ed. 2009, 48, 650-658.
- (5) Croissant, J. G.; Fatieiev, Y.; Almalik, A.; Khashab, N. M. Mesoporous Silica and Organosilica Nanoparticles: Physical Chemistry, Biosafety, Delivery Strategies, and Biomedical Applications. Adv. Healthcare Mater. 2018, 7, 1700831.
- (6) Noureddine, A.; Brinker, C. J. Pendant/Bridged/Mesoporous Silsesquioxane Nanoparticles: Versatile and Biocompatible Platforms for Smart Delivery of Therapeutics. Chem. Eng. J. 2018, 340, 125-
- (7) Vivero-Escoto, J. L.; Huxford-Phillips, R. C.; Lin, W. Silica-Based Nanoprobes for Biomedical Imaging and Theranostic Applications. Chem. Soc. Rev. 2012, 41, 2673-2685.
- (8) Croissant, J. G.; Cattoën, X.; Durand, J.-O.; Man, M. W. C.; Khashab, N. M. Organosilica Hybrid Nanomaterials with a High Organic Content: Syntheses and Applications of Silsesquioxanes. Nanoscale 2016, 8, 19945-19972.
- (9) Rocca, J. D.; Werner, M. E.; Kramer, S. A.; Huxford-Phillips, R. C.; Sukumar, R.; Cummings, N. D.; Vivero-Escoto, J. L.; Wang, A. Z.; Lin, W. Polysilsesquioxane Nanoparticles for Triggered Release of Cisplatin and Effective Cancer Chemoradiotherapy. Nanomedicine **2015**, 11, 31-38.
- (10) Vivero-Escoto, J. L.; Rieter, W. J.; Lau, H.; Huxford-Phillips, R. C.; Lin, W. Biodegradable Polysilsesquioxane Nanoparticles as

- Efficient Contrast Agents for Magnetic Resonance Imaging. Small 2013, 9, 3523-3531.
- (11) Croissant, J. G.; Mauriello-Jimenez, C.; Maynadier, M.; Cattoën, X.; Man, M. W. C.; Raehm, L.; Mongin, O.; Blanchard-Desce, M.; Garcia, M.; Gary-Bobo, M.; Maillard, P.; Durand, J.-O. Synthesis of Disulfide-Based Biodegradable Bridged Silsesquioxane Nanoparticles for Two-Photon Imaging and Therapy of Cancer Cells. Chem. Commun. 2015, 51, 12324-12327.
- (12) Croissant, J.; Maynadier, M.; Mongin, O.; Hugues, V.; Blanchard-Desce, M.; Chaix, A.; Cattoën, X.; Man, M. W. C.; Gallud, A.; Gary-Bobo, M.; Garcia, M.; Raehm, L.; Durand, J.-O. Enhanced Two-Photon Fluorescence Imaging and Therapy of Cancer Cells via Gold@Bridged Silsesquioxane Nanoparticles. Small 2015, 11, 295-299.
- (13) Mauriello Jimenez, C.; Aggad, D.; Croissant, J. G.; Tresfield, K.; Laurencin, D.; Berthomieu, D.; Cubedo, N.; Rossel, M.; Alsaiari, S.; Anjum, D. H.; Sougrat, R.; Roldan-Gutierrez, M. A.; Richeter, S.; Oliviero, E.; Raehm, L.; Charnay, C.; Cattoën, X.; Clément, S.; Man, M. W. C.; Maynadier, M.; Chaleix, V.; Sol, V.; Garcia, M.; Gary-Bobo, M.; Khashab, N. M.; Bettache, N.; Durand, J.-O. Porous Porphyrin-Based Organosilica Nanoparticles for NIR Two-Photon Photodynamic Therapy and Gene Delivery in Zebrafish. Adv. Funct. Mater. 2018, 28, 1800235.
- (14) Fatieiev, Y.; Croissant, J. G.; Julfakyan, K.; Deng, L.; Anjum, D. H.; Gurinov, A.; Khashab, N. M. Enzymatically Degradable Hybrid Organic-Inorganic Bridged Silsesquioxane Nanoparticles for In Vitro Imaging. Nanoscale 2015, 7, 15046-50.
- (15) Vega, D. L.; Lodge, P.; Vivero-Escoto, J. L. Redox-Responsive Porphyrin-Based Polysilsesquioxane Nanoparticles for Photodynamic Therapy of Cancer Cells. Int. J. Mol. Sci. 2016, 17, 56.
- (16) Vivero-Escoto, J. L.; De Cillis, D.; Fritts, L.; Vega, D. L. Porphyrin-Based Polysilsesquioxane Nanoparticles to Improve Photodynamic Therapy for Cancer Treatment. Proc. SPIE 2014, 8931, 89310Z.
- (17) Vivero-Escoto, J. L.; Vega, D. L. Stimuli-Responsive Protoporphyrin IX Silica-Based Nanoparticles for Photodynamic Therapy In Vitro. RSC Adv. 2014, 4, 14400-14407.
- (18) Kalimutho, M.; Parsons, K.; Mittal, D.; López, J. A.; Srihari, S.; Khanna, K. K. Targeted Therapies for Triple-Negative Breast Cancer: Combating a Stubborn Disease. Trends Pharmacol. Sci. 2015, 36, 822-846.
- (19) Khosravi-Shahi, P.; Cabezón-Gutiérrez, L.; Custodio-Cabello, S. Metastatic Triple Negative Breast Cancer: Optimizing Treatment Options, New and Emerging Targeted Therapies. Asia-Pac. J. Clin. Onco. 2017, 14, 32-39.
- (20) Nunez, C.; Capelo, J. L.; Igrejas, G.; Alfonso, A.; Botana, L. M.; Lodeiro, C. An Overview of the Effective Combination Therapies for the Treatment of Breast Cancer. Biomaterials 2016, 97, 34-50.
- (21) Darvishi, B.; Farahmand, L.; Majidzadeh-A, K. Stimuli-Responsive Mesoporous Silica NPs as Non-viral Dual siRNA/ Chemotherapy Carriers for Triple Negative Breast Cancer. Mol. Ther.-Nucleic Acids 2017, 7, 164-180.
- (22) Wu, X.; Wu, M.; Zhao, J. X. Recent Development of Silica Nanoparticles as Delivery Vectors for Cancer Imaging and Therapy. Nanomedicine. 2014, 10, 297-312.
- (23) Kumar, P.; Tambe, P.; Paknikar, K. M.; Gajbhiye, V. Mesoporous Silica Nanoparticles as Cutting-Edge Theranostics: Advancement from Merely a Carrier to Tailor-Made Smart Delivery Platform. J. Controlled Release 2018, 287, 35-57.
- (24) Yan, L.; Miller, J.; Yuan, M.; Liu, J. F.; Busch, T. M.; Tsourkas, A.; Cheng, Z. Improved Photodynamic Therapy Efficacy of Protoporphyrin IX-Loaded Polymeric Micelles Using Erlotinib Pretreatment. Biomacromolecules 2017, 18, 1836-1844.
- (25) Saito, G.; Swanson, J. A.; Lee, K. D. Drug Delivery Strategy Utilizing Conjugation via Reversible Disulfide Linkages: Role and Site of Cellular Reducing Activities. Adv. Drug Delivery Rev. 2003, 55, 199-215.

- (26) Panda, A. K.; Chakraborty, D.; Sarkar, I.; Khan, T.; Sa, G. New Insights into Therapeutic Activity and Anticancer Properties of Curcumin. *J. Exp. Pharmacol.* **2017**, *9*, 31–45.
- (27) Mock, C. D.; Jordan, B. C.; Selvam, C. Recent Advances of Curcumin and its Analogues in Breast Cancer Prevention and Treatment. *RSC Adv.* **2015**, *5*, 75575–75588.
- (28) Guan, F.; Ding, Y.; Zhang, Y.; Zhou, Y.; Li, M.; Wang, C. Curcumin Suppresses Proliferation and Migration of MDA-MB-231 Breast Cancer Cells through Autophagy-Dependent Akt Degradation. *PLoS One* **2016**, *11*, No. e0146553.
- (29) Adams, D.; Gonzalez-Duarte, A.; O'Riordan, W. D.; Yang, C.-C.; Ueda, M.; Kristen, A. V.; Tournev, I.; Schmidt, H. H.; Coelho, T.; Berk, J. L.; Lin, K.-P.; Vita, G.; Attarian, S.; Planté-Bordeneuve, V.; Mezei, M. M.; Campistol, J. M.; Buades, J.; III Brannagan, T. H.; Kim, B. J.; Oh, J.; Parman, Y.; Sekijima, Y.; Hawkins, P. N.; Solomon, S. D.; Polydefkis, M.; Dyck, P. J.; Gandhi, P. J.; Goyal, S.; Chen, J.; Strahs, A. L.; Nochur, S. V.; Sweetser, M. T.; Garg, P. P.; Vaishnaw, A. K.; Gollob, J. A.; Suhr, O. B. Patisiran, an RNAi Therapeutic, for Hereditary Transthyretin Amyloidosis. N. Engl. J. Med. 2018, 379, 11–21.
- (30) Rose, S. D.; Kim, D.-H.; Amarzguioui, M.; Heidel, J. D.; Collingwood, M. A.; Davis, M. E.; Rossi, J. J.; Behlke, M. A. Functional Polarity is Introduced by Dicer Processing of Short Substrate RNAs. *Nucleic Acids Res.* **2005**, 33, 4140–4156.
- (31) Xu, Z.; Xu, T.; Cheng, Y.; Ma, M.; Xu, P.; Qu, H.; Wen, L. Colorimetric Determination of Polyamidoamine Dendrimers and their Derivates Using a Simple and Rapid Ninhydrin Assay. *Anal. Lett.* **2008**, *41*, 444–455.
- (32) Aranda, A.; Sequedo, L.; Tolosa, L.; Quintas, G.; Burello, E.; Castell, J. V.; Gombau, L. Dichloro-Dihydro-Fluorescein Diacetate (DCFH-DA) Assay: A Quantitative Method for Oxidative Stress Assessment of Nanoparticle-Treated Cells. *Toxicol. In Vitro* **2013**, 27, 954–963.
- (33) Kim, Y. R.; Kim, S.; Choi, J. W.; Choi, S. Y.; Lee, S. H.; Kim, H.; Hahn, S. K.; Koh, G. Y.; Yun, S. H. Bioluminescence-Activated Deep-Tissue Photodynamic Therapy of Cancer. *Theranostics* **2015**, *5*, 805–817.
- (34) Wu, Y.; Wang, W.; Chen, Y.; Huang, K.; Shuai, X.; Chen, Q.; Li, X.; Lian, G. The Investigation of Polymer-siRNA Nanoparticle for Gene Therapy of Gastric Cancer In Vitro. *Int. J. Nanomed.* **2010**, *5*, 129–136.
- (35) Ganguli, A. K.; Ganguly, A.; Vaidya, S. Microemulsion-Based Synthesis of Nanocrystalline Materials. *Chem. Soc. Rev.* **2010**, 39, 474–485.
- (36) Mirzaei, H.; Khoi, M. J. M.; Azizi, M.; Goodarzi, M. Can Curcumin and its Analogs be a New Treatment Option in Cancer Therapy? *Cancer Gene Ther.* **2016**, 23, 410–419.
- (37) Nagaraju, G. P.; Aliya, S.; Zafar, S. F.; Basha, R.; Diaz, R.; El-Rayes, B. F. The Impact of Curcumin on Breast Cancer. *Integr. Biol.* **2012**, *4*, 996–1007.
- (38) Zaman, M. S.; Chauhan, N.; Yallapu, M. M.; Gara, R. K.; Maher, D. M.; Kumari, S.; Sikander, M.; Khan, S.; Zafar, N.; Jaggi, M.; Chauhan, S. C. Curcumin Nanoformulation for Cervical Cancer Treatment. *Sci. Rep.* **2016**, *6*, 20051.
- (39) Yallapu, M. M.; Khan, S.; Maher, D. M.; Ebeling, M. C.; Sundram, V.; Chauhan, N.; Ganju, A.; Balakrishna, S.; Gupta, B. K.; Zafar, N.; Jaggi, M.; Chauhan, S. C. Anti-Cancer Activity of Curcumin Loaded Nanoparticles in Prostate Cancer. *Biomaterials* **2014**, *35*, 8635–8648.
- (40) Yallapu, M. M.; Jaggi, M.; Chauhan, S. C. Curcumin Nanomedicine: a Road to Cancer Therapeutics. *Curr. Pharm. Des.* **2013**, *19*, 1994–2010.
- (41) McBain, S. C.; Yiu, H. H. P.; El Haj, A.; Dobson, J. Polyethyleneimine Functionalized Iron Oxide Nanoparticles as Agents for DNA Delivery and Transfection. *J. Mater. Chem.* **2007**, 17, 2561–2565.
- (42) Rosenholm, J. M.; Penninkangas, A.; Linden, M. Amino-Functionalization of Large-Pore Mesoscopically Ordered Silica by a

- One-Step Hyperbranching Polymerization of a Surface-Grown Polyethyleneimine. *Chem. Commun.* **2006**, 3909–3911.
- (43) Moghimi, S. M.; Hunter, A. C.; Murray, J. C. Long-Circulating and Target-Specific Nanoparticles: Theory to Practice. *Pharmacol. Rev.* **2001**, *53*, 283–318.
- (44) Xie, J.; Xu, C.; Kohler, N.; Hou, Y.; Sun, S. Controlled PEGylation of Monodisperse Fe3O4 Nanoparticles for Reduced Non-Specific Uptake by Macrophage Cells. *Adv. Mater.* **2007**, *19*, 3163–3166.
- (45) Hu, L.-C.; Khiterer, M.; Huang, S.-J.; Chan, J. C. C.; Davey, J. R.; Shea, K. J. Uniform, Spherical Bridged Polysilsesquioxane Nanoand Microparticles by a Non-emulsion Method. *Chem. Mater.* **2010**, 22, 5244–5250.
- (46) Khiterer, M.; Shea, K. J. Spherical, Monodisperse, Functional Bridged Polysilsesquioxane Nanoparticles. *Nano Lett.* **2007**, *7*, 2684–2687
- (47) Wang, D.; Niu, L.; Qiao, Z.-Y.; Cheng, D.-B.; Wang, J.; Zhong, Y.; Bai, F.; Wang, H.; Fan, H. Synthesis of Self-Assembled Porphyrin Nanoparticle Photosensitizers. *ACS Nano* **2018**, *12*, 3796–3803.
- (48) Lee, S. J.; Koo, H.; Lee, D.-E.; Min, S.; Lee, S.; Chen, X.; Choi, Y.; Leary, J. F.; Park, K.; Jeong, S. Y.; Kwon, I. C.; Kim, K.; Choi, K. Tumor-Homing Photosensitizer-Conjugated Glycol Chitosan Nanoparticles for Synchronous Photodynamic Imaging and Therapy Based on Cellular On/Off System. *Biomaterials* **2011**, *32*, 4021–4029.
- (49) Harigae, T.; Nakagawa, K.; Miyazawa, T.; Inoue, N.; Kimura, F.; Ikeda, I.; Miyazawa, T. Metabolic Fate of Poly-(Lactic-co-Glycolic Acid)-Based Curcumin Nanoparticles Following Oral Administration. *Int. J. Nanomed.* **2016**, *11*, 3009–3022.
- (50) Tang, Q.; Yu, B.; Gao, L.; Cong, H.; Song, N.; Lu, C. Stimuli Responsive Nanoparticles for Controlled Anti-cancer Drug Release. *Curr. Med. Chem.* **2018**, *25*, 1837–1866.
- (51) Siafaka, P. I.; Oku, N. U.; Karavas, E.; Bikiaris, D. N. Surface Modified Multifunctional and Stimuli Responsive Nanoparticles for Drug Targeting: Current Status and Uses. *Int. J. Mol. Sci.* **2016**, *17*, 1440.
- (52) Hadipour Moghaddam, S. P.; Saikia, J.; Yazdimamaghani, M.; Ghandehari, H. Redox-Responsive Polysulfide-Based Biodegradable Organosilica Nanoparticles for Delivery of Bioactive Agents. ACS Appl. Mater. Interfaces 2017, 9, 21133–21146.
- (53) Schafer, F. Q.; Buettner, G. R. Redox Environment of the Cell as Viewed Through the Redox State of the Glutathione Disulfide/Glutathione Couple. *Free Radical Biol. Med.* **2001**, *30*, 1191–1212.
- (54) Croissant, J. G.; Fatieiev, Y.; Khashab, N. M. Degradability and Clearance of Silicon, Organosilica, Silsesquioxane, Silica Mixed Oxide, and Mesoporous Silica Nanoparticles. *Adv. Mater.* **2017**, *29*, 1604634.
- (55) Bonnett, R.; Martinez, G. Photobleaching of Sensitisers Used in Photodynamic Therapy. *Tetrahedron* **2001**, *57*, 9513–9547.
- (56) Plaetzer, K.; Krammer, B.; Berlanda, J.; Berr, F.; Kiesslich, T. Photophysics and Photochemistry of Photodynamic Therapy: Fundamental Aspects. *Lasers Med Sci* **2009**, *24*, 259–268.
- (57) Karunagaran, D.; Rashmi, R.; Kumar, T. R. S. Induction of Apoptosis by Curcumin and its Implications for Cancer Therapy. *Curr. Cancer Drug Targets* **2005**, *5*, 117–129.
- (58) Huang, Z. A Review of Progress in Clinical Photodynamic Therapy. *Technol. Cancer Res. Treat.* **2005**, *4*, 283–293.
- (59) Khorsandi, K.; Hosseinzadeh, R.; Shahidi, F. K. Photodynamic Treatment with Anionic Nanoclays Containing Curcumin on Human Triple-Negative Breast Cancer Cells: Cellular and Biochemical Studies. *J. Cell. Biochem.* **2018**, *120*, 4998–5009.
- (60) Khopde, S. M.; Indira Priyadarsini, K.; Palit, D. K.; Mukherjee, T. Effect of Solvent on the Excited-State Photophysical Properties of Curcumin. *Photochem. Photobiol.* **2000**, *72*, 625–631.
- (61) Jalde, S. S.; Chauhan, A. K.; Lee, J. H.; Chaturvedi, P. K.; Park, J.-S.; Kim, Y. W. Synthesis of Novel Chlorin e6-Curcumin Conjugates as Photosensitizers for Photodynamic Therapy Against Pancreatic Carcinoma. *Eur. J. Med. Chem.* **2018**, *147*, 66–76.
- (62) Khan, A. A.; Quigley, J. G. Control of Intracellular Heme Levels: Heme Transporters and Heme Oxygenases. *Biochim. Biophys. Acta* **2011**, *1813*, 668–682.

- (63) Ruiz-González, R.; Bresolí-Obach, R.; Gulías, Ó.; Agut, M.; Savoie, H.; Boyle, R. W.; Nonell, S.; Giuntini, F. NanoSOSG: a Nanostructured Fluorescent Probe for the Detection of Intracellular Singlet Oxygen. *Angew. Chem., Int.Ed.* **2017**, *56*, 2885–2888.
- (64) Kim, S.; Fujitsuka, M.; Majima, T. Photochemistry of Singlet Oxygen Sensor Green. J. Phys. Chem. B 2013, 117, 13985–13992.
- (65) Gomes, A.; Fernandes, E.; Lima, J. L. F. C. Fluorescence Probes Used for Detection of Reactive Oxygen Species. *J. Biochem. Biophys. Methods* **2005**, *65*, 45–80.
- (66) Rackley, L.; Stewart, J. M.; Salotti, J.; Krokhotin, A.; Shah, A.; Halman, J. R.; Juneja, R.; Smollett, J.; Lee, L.; Roark, K.; Viard, M.; Tarannum, M.; Vivero-Escoto, J.; Johnson, P. F.; Dobrovolskaia, M. A.; Dokholyan, N. V.; Franco, E.; Afonin, K. A. RNA Fibers as Optimized Nanoscaffolds for siRNA Coordination and Reduced Immunological Recognition. *Adv. Funct. Mater.* **2018**, 28, 1805959.
- (67) Halman, J. R.; Satterwhite, E.; Roark, B.; Chandler, M.; Viard, M.; Ivanina, A.; Bindewald, E.; Kasprzak, W. K.; Panigaj, M.; Bui, M. N.; Lu, J. S.; Miller, J.; Khisamutdinov, E. F.; Shapiro, B. A.; Dobrovolskaia, M. A.; Afonin, K. A. Functionally-Interdependent Shape-Switching Nanoparticles with Controllable Properties. *Nucleic Acids Res.* **2017**, *45*, 2210–2220.
- (68) Afonin, K. A.; Grabow, W. W.; Walker, F. M.; Bindewald, E.; Dobrovolskaia, M. A.; Shapiro, B. A.; Jaeger, L. Design and Self-Assembly of siRNA-Functionalized RNA Nanoparticles for Use in Automated Nanomedicine. *Nat. Protoc.* **2011**, *6*, 2022–2034.
- (69) Nguyen, J.; Szoka, F. C. Nucleic Acid Delivery: the Missing Pieces of the Puzzle? Acc. Chem. Res. 2012, 45, 1153–1162.
- (70) Pasparakis, G.; Manouras, T.; Vamvakaki, M.; Argitis, P. Harnessing Photochemical Internalization with Dual Degradable Nanoparticles for Combinatorial Photo-Chemotherapy. *Nat. Commun.* **2014**, *5*, 3623.